LARGE EDDY SIMULATION OF BLUFF BODY STABILIZED FLAME WITH TURBULENT PREMIXED FLAME

Nicolas M. Cruz Salvador

Combustion and propulsion Laboratory (LCP)/INPE,
Rod. Presidente Dutra Km. 40 Cachoeira Paulista – SP – CEP 12630-000,
+55 (12) 3186-9500,
nmc.salvador@gmail.com

Marcio Texeira Mendonça

Institute of Aeronautics and Space (IAE),
Praça Mal. Eduardo Gomes 50 Vila das Acácias São José dos Campos – SP – CEP 12228-904,
+55 (12) 3947-5214,
marciomtm@iae.cta.br

Wladimyr Mattos da Costa Dourado

Institute of Aeronautics and Space(IAE),
Praça Mal. Eduardo Gomes 50 Vila das Acácias São José dos Campos – SP – CEP 12228-904,
+55 (12) 3947-4717,
wladimyrwmcd@iae.cta.br

Abstract: *The experimental results of a turbulent reacting flow in a channel with an obstacle was simulated computationally with large eddy simulation turbulence modeling, and the combustion Xi turbulent model for premixed flame. These numerical model is implemented in the open source package OpenFoam. Both inert flow and reactive flow simulations were performed. In the inert flow, comparisons with velocity profile and recirculation vortex zone in unsteady flow, as well as an analysis of the energy spectrum obtained numerically was performed. The spectrum was obtained in order to confirm if the mesh size is adequate for the turbulence model adopted. The simulation with reacting flow considered a pre-mixture of propane (C3H8) and air such that the equivalence ratio was equal to 0.65, with a theoretical adiabatic flame temperature of 1800 K. The equivalence ratio, inflow velocity, pressure, flame-holder shape and size, fuel type and turbulence intensity were taken from an experimental set up described in the literature. The results shown in the present simulations are in good agreement with the experimental data.*

Keywords: *CFD, reacting flow, large eddy simulation, combustion modeling, flame surface density..*

1 Introduction

In the context of turbulent reactive flow simulations, computational models have achieved a great development in recent years with the improvement of computer power. This development allowed more accurate solution of problems such as the instability caused by the thermoacoustic coupling in combustion chambers of rocket engines and gas turbines.

In turbulent combustion the behavior of the turbulent flame front is predominantly dictated by the turbulence (Peters, 2000). Combustion instability is also directly related to turbulence (Weller H., 1990). Therefore it becomes mandatory that the turbulence model be able to reproduce these dynamic processes, which are mainly produced by large scale turbulence. Many researchers have used Reynolds Averaged Navier Stokes (RANS) and eddy viscosity turbulence models to simulate reactive flows behind bluff bodies. However important discrepancies were observed due to shortcomings in the RANS methodology, especially in complex flows (Bai, 2001; Dourado, 2003). In large eddy simulation (LES), the three dimensional large scale motion is resolved, hence the non-universal geometry dependent flow features are captured accurately and only the small scales that exhibit local isotropy are modelled.

Many experimental studies on bluff body stabilized flames have been carried out. Cheng *et al.* (1989), Cheng and Shepherd (1991), Cheng (1984), Sjunesson (1992), Sanquer (1998) conducted a series of measurements of premixed bluff body stabilized flames, focusing mostly on the aspects of flame-turbulence interactions. Various models for turbulent combustion were experimentally validated and assessed by Veinante *et al.* (1994, 1996) using bluff body flame stabilization techniques. Turbulent flame measurements in a bluff body stabilized premixed flame were also carried out by Fuji *et al.* (1978); Fuji and Eguchi (1981). Furthermore, Hertzberg *et al.* (1991), Dourado (2003) studied the vortical pattern behind bluff

bodies in reactive flow and the vortical interaction with the flame. Porumbel (2006) have simulated bluff body flows with the Linear Eddy Mixed (LEM) LES based on the model proposed by Kerstein (1989); Menon *et al.* (1993) for premixed combustion.

In this paper we present results of numerical simulations using LES in order to simulate inert and reactive flows an compare the results with experimental results obtained by Sanquer (1998). The two cases considered, reactive and inert, are flows in a channel of rectangular cross section with a triangular obstacle. The Reynolds number based on the side of the triangle is equal to 6690. The purpose of this study is to evaluate OpenFOAM, an open source computational fluid dynamics software, as a model to simulate turbulent inert and reactive flows. OpenFoam contains large eddy simulation turbulence models and premixed combustion models and it is proposed to compare the numerical results obtained with these models with experimental results obtained by Sanquer (1998).

2 Problem Formulation

In turbulent combustion the turbulence wrinkles and stretches the laminar flame sheet propagation, increasing the area the sheet and the effective flame speed. Usually the large turbulent eddies corrugate and wrinkle the flame sheet. Moreover small turbulent eddies, if they are smaller than the laminar flame thickness, penetrate the flame sheet and changes its structure.

In order to account for turbulence and combustion the reactive flow governing equations are filtered using the LES concept and the combustion process is accounted for by following the flame front. Therefore it is necessary to define the filtering and a variable to account for the regions of burned and unburned gases. In the following derivation the formulation derived by Weller H. (1993, 2004).

2.1 Preliminary Definitions

In premixed flames a reaction wave propagates from the burned to fresh gases. The progress variable c that identifies this propagation takes values between 0 for fresh gas and 1 for for burned gas. The transition between these values describe the flame front. A progress variable c can be defined based on the normalised temperature(T) or the reactant mass fraction(Y). Using temperature, results:

$$c = \frac{T - T_u}{T_b - T_u}. \tag{1}$$

Where b subscript stands for burned gas, and u subscript for fresh gases. The flame front propagation is modelled by solving a transport equation for the density-weighted mean reaction regress variable denoted by b, where $b = 1 - c$.

In LES it is assumed that the dependent variables can be divided into grid scale (GS) and sub-grid scale (SGS) components, such that for a any given dependent variable ψ results:

$$\psi = \overline{\psi} + \psi^{'}. \tag{2}$$

Where

$$\overline{\psi} = G * \psi = \int_D G(\mathbf{x}^{'}, \Delta)\psi(\mathbf{x}^{'}, t)d^3\mathbf{x}^{'} \tag{3}$$

Here D is the computational domain with boundaries ∂D. The kernel $G = G(\mathbf{x}, \Delta)$ is any function of $\mathbf{x}$ and of the filter width Δ. G has the properties $\int_D G(\mathbf{x})d^3x = 1$, $\lim_{\Delta\to 0} G(x, \Delta) = \delta(x)$ and $G(x, \Delta) \in C^n(\mathrm{R}^3)$.

Introducing a "conditional filter" (Weller H., 2004), with an indicator function l such that:

$$l(\mathbf{x}, t) = \begin{matrix} 1 & \text{if}(\mathbf{x}, t)\text{is in phase A (unburnted gas)} \\ 0 & \text{otherwise.} \end{matrix} \tag{4}$$

For a tensor ψ of any rank, one may define $\overline{\overline{\psi}}$ the phase-weighted value of ψ at any point.

$$\overline{\overline{\psi}} = G * (l\psi) = \int_D G(\mathbf{x} - \mathbf{x}^{'}) l(\mathbf{x}^{'}, t) \psi(\mathbf{x}^{'}, t) d^3 x^{'}, \tag{5}$$

Introducing the combustion progress variable $\overline{b}$ as a GS indicator function such that

$$\overline{\overline{\psi}} = \overline{b}\ \overline{\psi_u}, \tag{6}$$

where $\overline{b}(x,t)$ is the probability of the point $(\mathbf{x}, t)$ being in the unburnt gas.

$$\overline{b} = \int_D G(\mathbf{x} - \mathbf{x}^{'}) l(\mathbf{x}^{'}, t) d^3 \mathbf{x}^{'}. \tag{7}$$

In compressible flow we need density variation and the product $\overline{\overline{\rho\psi}}$ can be written:

$$\overline{\overline{\rho\psi}} = \overline{b}\ \overline{\rho\psi_u}. \tag{8}$$

Where the subscript u indicates the unburned phase. Defining a density-weight average $\widetilde{\psi}_u$ in the unburned phase to split up this second term:

$$\overline{\rho\psi_u} = \overline{\rho_u}\widetilde{\psi_u}, \tag{9}$$

Equation 9 in 8, results:

$$\overline{\overline{\rho\psi}} = \overline{b}\ \overline{\rho}\widetilde{\psi_u}. \tag{10}$$

2.2 Continuity Filtered Equation

The governing equations will be written in a coordinate system placed at the flame surface, such that $\mathbf{n}_\perp$ and $\mathbf{n}_\parallel$ are the unity vectors pointing the normal $x_\perp$ and parallel $x_\parallel$ directions to the flame surface. The metrics of this coordinate system are $h_\perp$ and $h_\parallel$. This coordinate system is used in order to include the conditional filter based on the progress variable b.

The filtered continuity equation reads (Weller H., 2004):

$$\frac{\partial \overline{\rho}}{\partial t} + \nabla \cdot \overline{\overline{\rho \mathbf{U}}} = \overbrace{\overline{\rho(\mathbf{U} - \mathbf{U}_I) \cdot \mathbf{n}_\perp}}^{\sum}. \tag{11}$$

Where $U_I = U + v_a n_\perp$, U_I is the full velocity on an interface consisting of the movement due to advection term U and the advance of the interface relative to the flow $v_a n_\perp$.

In the transformed coordinates for $(x_\perp, x_\parallel)$:

$$\sum = G_\perp(x_\perp - x_{\perp,I}) \int\int G_\parallel(\mathbf{x}_\parallel - \mathbf{x}_\parallel^{'}) |\mathcal{J}| d^2 \mathbf{x}_\parallel^{'}, \tag{12}$$

and $\mathcal{J}$ represents the Jacobian of the transformation. $|\mathcal{J}|d^2\mathbf{x}_{\|}^{'}$ is the area element on the surface interface. $\sum$ is interpreted as the amount of interface for the filtered component.

The surface filtering operation $\widetilde{\ }$ is defined as

$$\widetilde{\psi} = \frac{1}{\sum}\int_D G(\mathbf{x}-\mathbf{x}^{'})\psi(\mathbf{x}^{'})\delta((\mathbf{x}^{'}-\mathbf{x})n_{\perp})\frac{1}{h_{\perp}}d^3\mathbf{x}^{'} \tag{13}$$

From 9 in 11 result:

$$\frac{\partial\bar{b}\overline{\rho_u}}{\partial t} + \nabla\cdot\bar{b}\overline{\rho_u}\widetilde{U_u} = -\widetilde{\rho v_a}\sum. \tag{14}$$

From 13 filtred for $\mathbf{n}_{\perp}$ result:

$$\widetilde{n_{\perp}} = \frac{1}{\sum}G_{\perp}(x_{\perp}-x_{\perp,I})\int\int G_{\|}(\mathbf{x}_{\|}-\mathbf{x}_{\|}^{'})\mathbf{n}_{\perp}((\mathbf{x}_{\perp,I},\mathbf{x}_{\|}^{'})|\mathcal{J}|d^2\mathbf{x}_{\|}^{'}, \tag{15}$$

How $\tilde{b}$ measure the large-scale geometry of the surface, $\widetilde{n_{\perp}}$ also can be related to the GS with the $\mathbf{n_f}$ direction of the interface.

$$\widetilde{n_{\perp}} = \frac{n_f}{\Xi} \tag{16}$$

where Ξ represent the total subgrid surface area by the smoothed surface area in the $\mathbf{n_f}$ direction:

$$\Xi = \frac{1}{|\widetilde{n_{\perp}}|} = \frac{\sum}{|G_{\perp}(x_{\perp}-x_{\perp,I})\int\int G_{\|}(\mathbf{x}_{\|}-\mathbf{x}_{\|}^{'})\mathbf{n}_{\perp}((\mathbf{x}_{\perp,I},\mathbf{x}_{\|}^{'})|\mathcal{J}|d^2\mathbf{x}_{\|}^{'}|}, \tag{17}$$

From the equation of identity filtered and substituting in 17, result:

$$\Xi = \frac{\sum}{|\nabla\bar{b}|} \tag{18}$$

where $|\nabla\bar{b}|$ represent the area of the GS surface.

2.3 Momentum, Energy equations

Introducing the conditional filtering in the momentum equation gives

$$\frac{\partial(\bar{b}\overline{\rho_u}\widetilde{U_u})}{\partial t} + \nabla.(\bar{b}\overline{\rho_u}\widetilde{U_u}\otimes\widetilde{U_u}) = -\nabla\bar{b}\overline{p_u} + \nabla.\left\{\bar{b}(\overline{S_u}-B_u)\right\} + [\widetilde{(pI-S).n_{\perp}} - \widetilde{\rho v_a U}]\sum. \tag{19}$$

Where p is the pressure, S_u is the laminar flame speed, $\sum$ the flame surface density, $S = \lambda\nabla.UI + 2\mu D$ and $D = \frac{1}{2}(\nabla U + \nabla U^T)$.

$$\mathbf{B_u} = \overline{(\rho\mathbf{U}\otimes\mathbf{U})}_u - \overline{\rho_u}\widetilde{\mathbf{U}}_u\otimes\widetilde{\mathbf{U}}_u. \tag{20}$$

$\mathbf{B}_u$ represent the SGS stress tensor and require modeling, the terms in brackets represent the effects of the interface on the moment balance.

The energy equation filtered is showed:

$$\frac{\partial(\overline{b}\overline{\rho_u}\widetilde{e_u})}{\partial t}++\nabla.(\overline{b}\overline{\rho_u}\widetilde{e_u}\widetilde{U_u} = -(\overline{b}\overline{p_u}\nabla.\widetilde{U_u}+\overline{b}\overline{\rho_u}\pi_u)+(\overline{bS_u}.D_u)+\overline{b}\overline{p_u}\epsilon_u)+\nabla.\overline{b}(\overline{h_u}-b_u)+[\widehat{\rho e v_a}-\widehat{h.n_\perp}]. \quad (21)$$

where

$$\overline{\rho_u}\pi_u) = \overline{(p\nabla.U)_u} - \overline{p_u}\nabla.\widetilde{U_u}, \quad (22)$$

$$\overline{\rho_u}\epsilon_u) = \overline{S.D)_u} - \overline{S_u}.\overline{D_u}, \quad (23)$$

represent the SGS pressure dilatation and dissipation π and ϵ (Weller H., 2004). The total energy in the interface is presented in brackets.

2.4 Transport equation

A model for the sub-grid scales (SGS) stress tensor, the flux vectors, the dissipation and filtered raction rates are used to close de governing equations. A flamelet model with conditional filtering for LES is used to generate transport equations that differ from conventional models. The conventional models use the flame propagations speed in terms of the laminar flame area per unit volume $\sum$ and the degree of wrinkling of the flame at a point in the domain. The model proposed by Weller H. (1993) represent the geometrics properties of the flame front in terms of the flame surface density used along with a surface function Ξ called wrinkling surface. The surface function Ξ is the average flame area per unit volume A_f devided by the projected area in the mean direction of propagation A_s, $\Xi = A_f/A_s$.

In the reaction zone the characteristic scales for the reaction processes are below the filter, so that in reacting LES a proper treatment (modeling) of the raction zone is needed.

Conditioning is applied to the continuity equation in order to consider unburnt and burnt gases separately. Transport equations for the resolved part of the mass fraction of unburned gas and burned gas are obtained. Subscript u refers to the unburned gas and the burned gas are considered through the regress variable $\tilde{b}$ Weller H. (1998). The velocity $\mathbf{v}$ is writen as $\mathbf{U}_I = \mathbf{U} + v_a n_\perp$, where $\mathbf{U}_I$ is the full velocity on an interface due to advection and the advance of the interface relative to the flow.

$$\frac{\partial\overline{\rho}\tilde{b}}{\partial t} + \nabla.(\overline{\rho}\tilde{U_u}\tilde{b}) = -\overline{\rho}_u S_u \Xi|\nabla\overline{b}|, \quad (24)$$

where $-$ and $\sim$ represent filtered and density weighted filtered variables respectively. The volume fraction of unburned gas $\overline{b}$ is related to $\tilde{b}$ through $\overline{\rho_u}\overline{b} = \overline{\rho}\tilde{b}$ and Ξ is the sub-grid flame wrinkle. The interface advance term $\widehat{\rho v_a}$ is modelled in terms of the laminar flame speed S_u and unburned gas density ρ_u.

The conditional filter of unburned gas velocity $\tilde{U_u}$ is modeled using $\tilde{U_u} = \tilde{U} + (1-\tilde{b})\overline{U}_{ub}$ where $\overline{U}_{ub}$ is the slip velocity of the unburned minus burned gas $\overline{U}_{ub} = \overline{U}_u - \overline{U}_b$. By analogy with the properties of laminar flame for LES:

$$\overline{U}_{ub} = (\frac{\overline{\rho}_u}{\overline{\rho}_b} - 1)S_u\Xi\hat{n} - D\frac{\nabla\tilde{b}}{\tilde{b}(1-\tilde{b})}. \quad (25)$$

Where D is the diffusion coefficient of the sub-grid, and $\hat{n} = \nabla\tilde{b}/|\nabla b|$ the flame normal. Combining equations (9) and (10) one arrive at the equation for $\tilde{b}$ (Weller H., 2004):

$$\frac{\partial\overline{\rho}\tilde{b}}{\partial t} + \nabla.(\overline{\rho}\tilde{U}\tilde{b}) - \nabla.(\overline{\rho}D\nabla\tilde{b}) = -\overline{\rho}_u S_u\Xi|\nabla\tilde{b}|. \quad (26)$$

From the transport equation for the sub-grid flame area density Σ proposed by (Weller H., 1993) is obtained from the relation $\Xi = \Sigma/|\nabla\overline{b}|$ and the resolved unburned gas volume fraction b:

$$\frac{\partial\Xi}{\partial t} + \widehat{U_s}.\nabla\Xi = -\overbrace{n.(\nabla U_s).n}\Xi + \hat{n}(\nabla\widehat{U_t})\hat{n}\Xi + (\widehat{U_t} - \widehat{U_s}).\frac{\nabla|\nabla b|}{|\nabla b|}\Xi. \quad (27)$$

Here $\widehat{U_t}$ is the surface-filtered effective velocity of the flame ($\partial\overline{b}/\partial t + \widehat{U_t}\nabla\overline{b} = 0$) and U_s is the local

instantaneous velocity of flame surface. The first and second term on the right hand side of equation (12) represent the effects of stress and propagation on the SGS of Ξ. The third term on the right hand side of equation (12) represent the effect of strain and differential propagation on Ξ through the flame, reducing the generation at the front of the flame and increasing the generation at the back. These terms involve higher order derivatives which are difficult to evaluate numerically for LES, so they are modeled. Instead of attempting to model each term in detail, models are used that represent the generation and removal of wrinkled (respectively by $G\Xi$ and $R(\Xi - 1)$). The problem associated with these derivatives is thus avoided by including the effect directly into the model for a given value of G, resulting in the following simplified equation for Ξ:

$$\frac{\partial \Xi}{\partial t} + \widehat{U_s}.\nabla\Xi = G\Xi - R(\Xi - 1) + (\sigma_s - \sigma_t)\Xi. \tag{28}$$

Here the final term may be correlated with the resolved strain rates:

$$\sigma_t = \frac{1}{2} \parallel \nabla \widehat{U_t} + \nabla \widehat{U_t}^T \parallel,$$

and

$$\sigma_t = \frac{1}{2} \parallel \nabla \widehat{U_I} + \nabla \widehat{U_I}^T \parallel .$$

A spectral approach is applied to the modeling of the interaction between turbulence and flame, in which the wrinkled flame front is represented by a distribution length-scale of distortions of the surface, limited by the size of the kernel flame and the thickness of the laminar flame (Weller H., 1990). However, the solution of the equations of spectral evolution coupled with the transport equations for Ξ is expensive and algebraic models are considered more appropriate. The approach used is based on the correlation of Gülder for flame speed (Gulder, 1990):

$$G = R\frac{\Xi_{eq} - 1}{\Xi_{eq}}, \; R = \frac{0.28}{\tau_\eta}\frac{\Xi^*_{eq} - 1}{\Xi^*_{eq}}, \tag{29}$$

which has proved particulary good with full expectral results.

$$\Xi^*_{eq} = 1 + 0.62\sqrt{\frac{u'}{S_u}}Re_\eta. \tag{30}$$

Or including the regress variable.

$$\Xi_{eq} = 1 + 2(1 - b)(\Xi^*_{eq} - 1). \tag{31}$$

Where τ_η is the Kolmogorov time, u' is the intensity of turbulence in the sub-grid and Re_η is the Reynolds number of Kolmogorov. It is assumed that the laminar flame speed is in balance with the rate of local deformation and in linear response, resulting:

$$S^\infty_u = S^0_u max(1 - \sigma_s/\sigma_{ext}, 0). \tag{32}$$

Where σ_{ext} is the strain rate at extinction. Unfortunately, the scales of chemical time of lean flame can be comparable to the time scales of deformation and transportation. Therefore the local equilibrium assumption is wrong, which requires a full transport equation to be used. By analogy with the transport of a wrinkled flame, it is expected that the filtered laminar flame speed is carried by the surface speed of filtered flame $\widehat{U_s}$. Assuming that the timescale of the strain rate is $1/\tau_s$ and the chemical time scale is such that, when $t \to \infty, Su \to S^\infty_u$ then:

$$\frac{\partial S_u}{\partial t} + \widehat{U_s}.\nabla S_u = -\sigma_s S_u + \sigma_s S^\infty_u \frac{(S^0_u - S_u)}{(S^0_u - S^\infty_u)}. \tag{33}$$

Thus, the wrinkled flame model can be simplified by replacing Ξ in equation (13) by the equilibrium expression (16) and also by substitution of expression (17) in equation (18).

3 Numerical Model

Explicit Euler's time discretization is used. For spatial discretization second and third order TVD (Total Variation Diminishing) schemes are used. The PISO algorithm (pressure-implicit split-operator) is used to solve the pressure-velocity coupling. The discretization method is the standard Gauss finite volume integration. The combustion solver called Xifoam available on openFoam was used. This premixed turbulent combustion model is described in Sec. 2.1 (Weller H., 1998, 2004).

3.1 Initial and boundary conditions

The model is presented in Fig. 1 and consists of a channel of 0.6 m long, 0.16 m wide and 0.00288 m tall, where the Reynolds number based on the inlet velocity and channel height, $Re = U_{axe}2h/\nu$ is 6600. The obstacle used as flame holder is an equilateral triangular cross section obstacle whose backside is located 160 cm from the entrance. The obstacle blockage is 33% of the total area and corresponds to r-65 test case in Sanquer's Thesis (Sanquer, 1998). Figure 1 shows the topology of the channel.

First only inert simulations are considered with an initial temperature of 300 K. At the outflow boundary a pressure wave transmissivity boundary condition is used for pressure (Candel, 1992). A turbulent velocity profile is imposed at the entrance with a speed of 3.1 m/s to match the experimental conditions as shown in Fig. 3 and 4. The flow is considered periodic in the spanwise direction. A wall function in the chanel and in the obstacle is used Jayatilleke (1969) fig. 4.

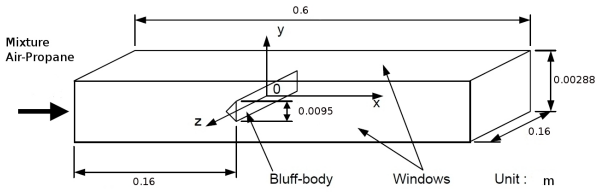

Figure 1: Scheme of Sanquer's experiment.

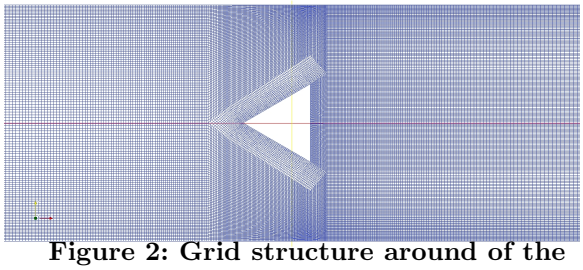

Figure 2: Grid structure around of the obstacle.

For reacting flows propane (C3H8) premixed with air is considered. The mixture is ignited behind the obstacle in the recirculation zone to achieve a proper performance and avoid flame blow off. The ignition point is located at 0.05 m behind the obstacle in the center of the recirculation zone. A combustion time of 3 miliseconds was used before colecting data to avoid numerial transients and allow time to achieve stable combustion behaviour. The imposed initial flame speed was 0.256 m/s and The initial condition for the regress variable was $b = 1$.

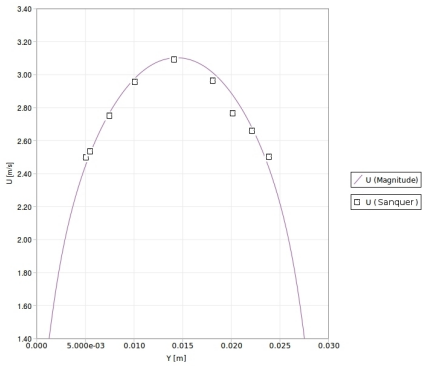

Figure 3: turbulent velocity profiles at the channel entrance, experimental and imposed boundary condition.

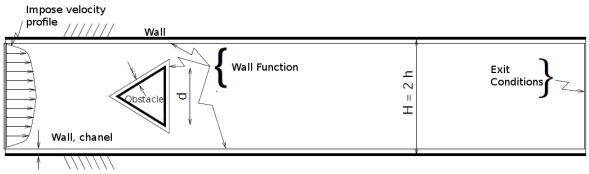

Figure 4: Schematic boundary conditions. Turbulent velocity profiles at the channel entrance, wall and obstacle.

The mesh presented in this paper is composed of 388,355 volumes for two-dimensional simulations and 2,300,000 volumes in 3D. Fig. 2 shows the mesh topology around the obstacle. For lower mesh densities, it was not possible to recover the recirculation zone size obtained by Sanquer (Sanquer, 1998)

The instantaneous velocity was monitored in order to stablish when the flow can be considere periodic stationary. Fig. 5 shows the history of longitudinal velocity. As can be seen the transition lasts 18 milliseconds, so the flow can be considered stationary periodically beyond that.

4 Results

The recirculation zone and the energy spectra are determined through the velocity measurement after the simulation reaches the stationary periodic state. Once the length of the recirculation zone Xr is determined, one can calculate the Strouhal number to compare with experimental results. To determine the values of the energy spectrum the Fast Fourier transform (FFT) of the oscillatory instantaneous

velocity is taken. This information is used to determine if the simulation capture the large turbulent scales and the sub-grid scales.

4.1 Inert flow case

The results show good agreement with those obtained experimentally as shown in Tab. 1. The length of recirculation zone based on the evolution of the average velocity Ux were determined taking the average values along the X axis downstream of the obstacle. The recirculation zone length differs approximately 11.5% from the experimental value. Figure 6 shows the profile of the average velocity used to define the recirculation zone as shown in 7. The length of the recirculation zone found in the present simulation is 0.023 m, while the length found by Sanquer (1998) is 0.0204 m.

Table 1: Comparison of numerical LES and RANS results with experimental results.

	$f_q[Hz]$	$f_q d/U_{axe}$	$\triangle Xr[m]$	Xr/d
Experimental Sanquer	89	0.276	0.0204	2.12
LES current work	93.5	0.284	0.023	2.42
RANS Dourado Dourado (2003)	87	0.2694	0.0222	2.31

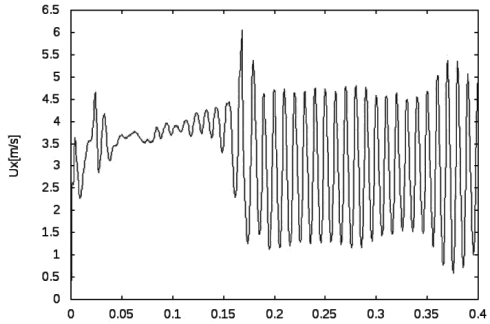

Figure 5: Evolution of velocity components Ux.

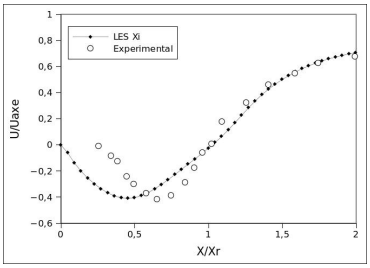

Figure 6: Profile of the average velocity $\tilde{u}$ in the recirculation zone.

To determine the vortex emission frequency a Fourier temporal analysis was used Dourado (2003). The value of 93.5 Hz was found as shown in fig. 8, corresponding to a Strouhal number $St = 0.284$. This value compares well with the experimental $St = 0.276$ value with a difference of only 3%.

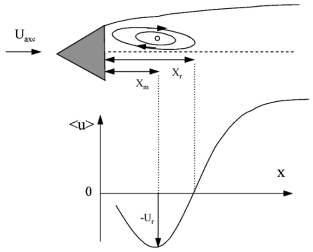

Figure 7: Schematic representation of the velocity distribution (Sanquer, 1998).

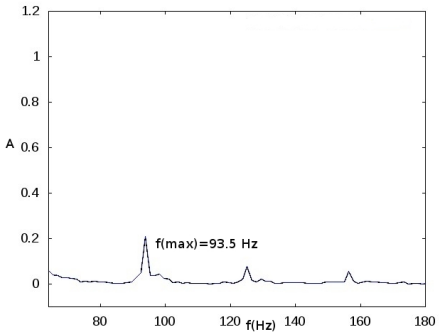

Figure 8: Frequency spectrum identifying the vortex emissions frequency.

Energy frequency spectrum are shown in Fig. 9 at two points for the longitudinal and normal components of velocity. As in the work of Sanquer (1998), these points are at $X/Xr = 1.4$; $y/h = 0$ and $X/Xr = 1.4$ and $y/h = 0.41$.

Considering the spanwise velocity component, the energy spectrum shown in 9 captures the -5/3 energy decay rate expected for a large Reynolds number turbulent flow on Figs. (e) and (f). This result shows that the mesh refinement is adequate for the present analysis. Figs (a) through (d) are two dimensional and a correct energy decay is not expected due to the supresion of large scales turbulence on the third dimension. The energy spectrum shown in 9 do not show very clearly the energy peaks corresponding to the large scale vortex shedding frequency. A peak of 80 Hz can be identified on Fig. 9 (f) and (g)

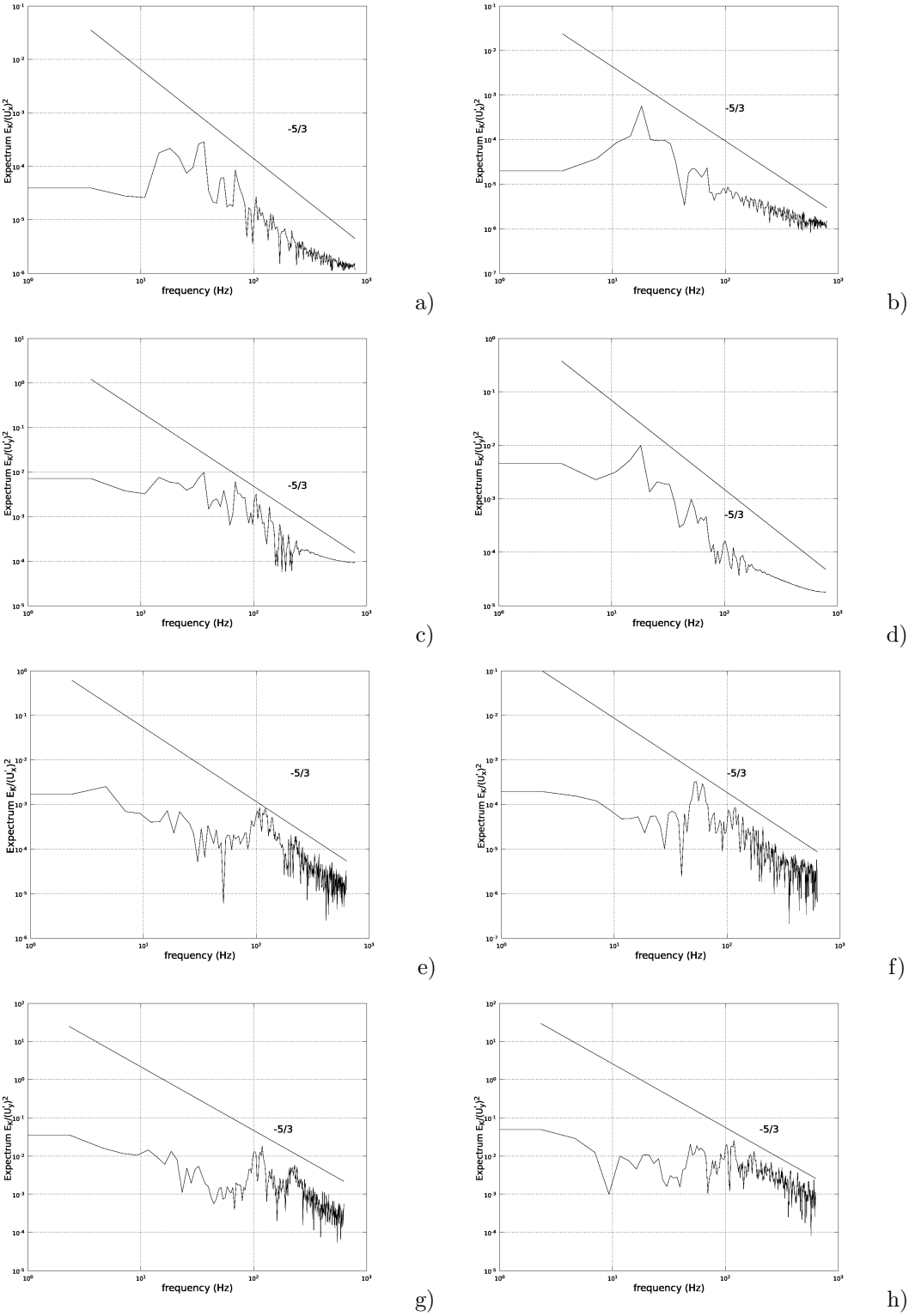

Figure 9: Energy spectrum of longitudinal and normal velocity components at (a) Ux**,** $X/Xr = 1.4$**,** $y/h = 0$**; (b)** Ux**,** $X/Xr = 1.4$**,** $y/h = 0.41$**; (c)** Uy**,** $X/Xr = 1.4$**,** $y/h = 0$**; (d)** Uy **in** $X/Xr = 1.4$**,** $y/h = 0.41$**; (e) 3-D** Ux**,** $X/Xr = 1.4$**,** $y/h = 0$**; (f) 3-D** Ux**;** $X/Xr = 1.4$**,** $y/h = 0.41$**; (g) 3-D** Uy**,** $X/Xr = 1.4$**,** $y/h = 0$**; (h) 3-D** Uy**,** $X/Xr = 1.4$**,** $y/h = 0.41$**.**

Filtered longitudinal Ux and normal Uy component velocity profiles at $X/Xr = 0.8$ and $X/Xr = 1.4$ are shown in fig. 10. The longitudinal velocity profile obtained in the simulation are close to the experimental velocity profiles in the recirculation zone. At $X/Xr = 1.4$ the longitudinal velocity distribution is underpredicted in the region between the recirculation zone and the wall. The simulation indicates a possible boundary layer separation on the wall due to the flow expansion behind the obstacle. Further investigations are underway to elucidate this behaviour.

Regarding the vertical velocity component Uy the numerical results capture the general trend observed experimentaly, but the velocity distribution is shifted upward at $X/Xr = 0.8$ and underpredicted at $X/Xr = 1.4$ at heights above the separation bubble. This behaviour should be related to the prediction of a separation bubble on the channel walls.

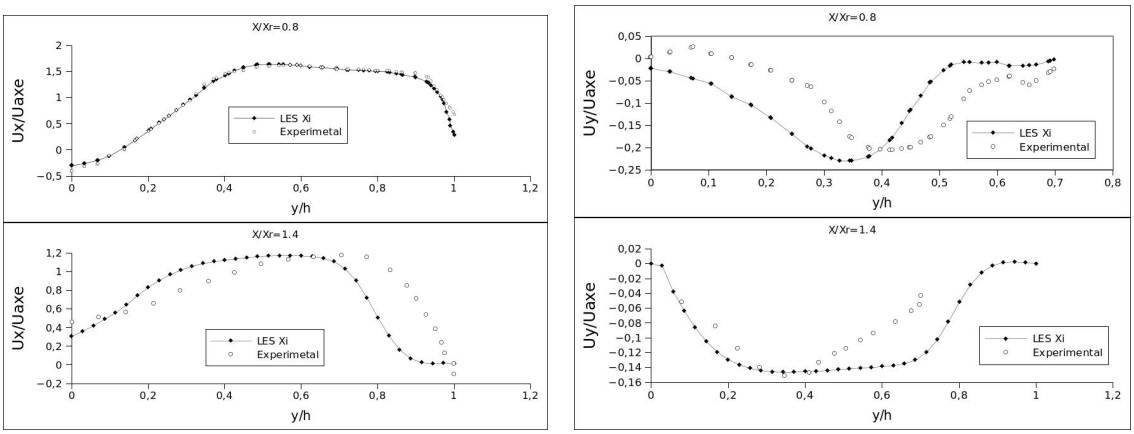

(a) (b)

Figure 10: Inert case. (a) Mean longitudinal component velocity profile Ux at $X/X_r = 0.8$ and $X/X_r = 1.4$ and (b) normal component velocity profile Uy at $X/X_r = 0.8$ and $X/X_r = 1.4$

4.2 Reactive case

For the 3D reactive case results are shown in Fig. 11, 12 and 13 for the simulations with the Smagorinsky turbulence model.

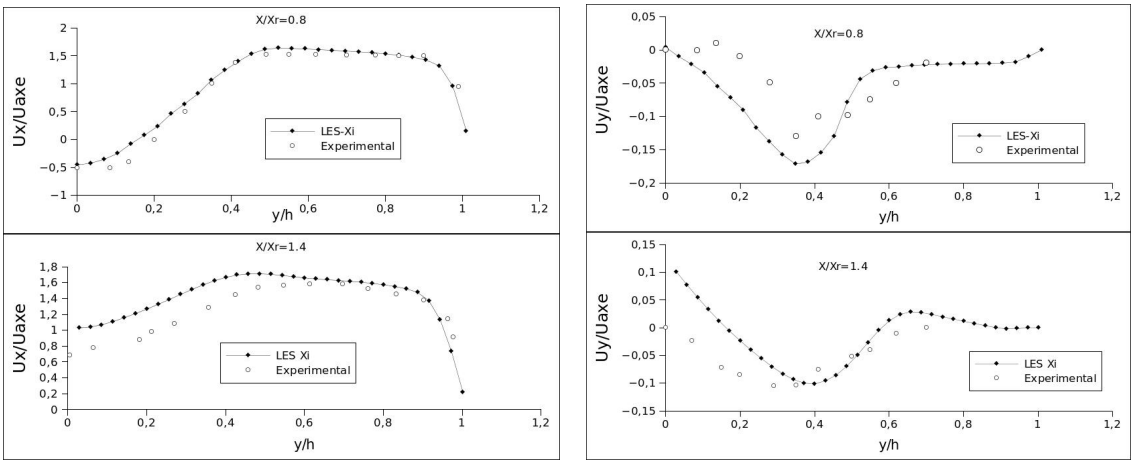

(a) (b)

Figure 11: Reactive case. (a) Mean longitudinal component velocity profile Ux at $X/X_r = 0.8$ and $X/X_r = 1.4$ and (b) normal component velocity profile Uy at $X/X_r = 0.8$ and $X/X_r = 1.4$

For the present study on the reactive flow, we compare the values obtained experimentally by Sanquer (Sanquer, 1998) for the case with a triangular dihedral with 33% of the channel blockage and with a equivalence ratio equal 0.65 referred to as r1-65 in his work.

As can be seen in Fig. 11, the profiles obtained in the simulation are close to the experimental profiles. At $X/X_r = 0.8$ the results are better than at $X/X_r = 1.4$ probably due to a higher turbulent intensity predominant downstream of the recirculation zone Porumbel (2006), both in the reactive and inert cases. The near zero shear stress at the upper wall present in the inert case is no longer observed indicating that no separation bubble on the channel walls are likely to appear. The values of normal velocity at $X/X_r = 0.8$ are slightly displaced in the simulation as in the inert case. However the highest and lowest Uy/U_{axe} (0 and -0.2) are within the limits of the experimental error. At $X/X_r = 1.4$ the behavior is different, the nearly constant velocity in the region $.2 < y/h < .7$ observed in Fig. 10 is no longer obtained and the profile is closer to the experimental profile. This is likely related to the products of the reactive process.

Another results is shown in Fig. 12 where the progress variable is presented. The simulation captures the general behaviour of the progess variable quite well. Despite the fact that the simulation underpredicts the progress variable inside the flame zone, the flame front at $c \approx 0.05$ around $y/h = .6$ matches the experimental value. Also, Sanquer (Sanquer, 1998) states that the experimental results seems to be displaced to the left.

For the 3D reactive case a value of 1750 K was obtained for the flame average temperature. The theoretical adiabatic flame temperature for a equivalence ratio of 0.65 corresponds to 1750 K for this fuel. Figure 13 shows the temperature distribution in the normal direction with a profile corresponding to a premixed flame.

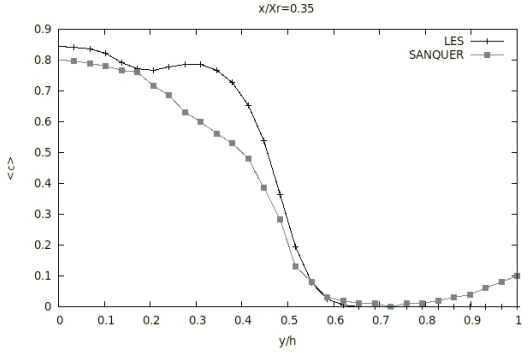

Figure 12: Profile of progress variable at $X/Xr = 0.35$.

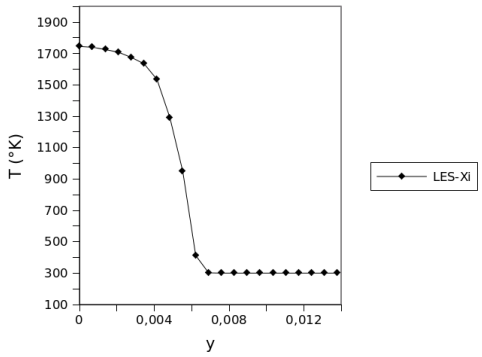

Figure 13: Mean temperature profile.

5 Conclusions

It was found that OpenFoam can reproduce the experimental data obtained by S. Sanquer and numerical solutions were obtained for 2 and 3 dimensions models. However the values of the energy spectra for 2-D is not expected to recover the physical value and was used only for development purposes. The values for the recirculation zone falls in the expected range and the Strouhal number is very close to that found in the experiment. These results are in agreement with the values obtained with a RANS models. The result for the 3-D simulation spectral analysis show the expected -5/3 decay and the energy peak corresponding to vortex sheading are not very sharply captured, but does correspond approximately to the experimental value. Considering the comparisons of the velocities with the experimental simulations, they are well approximated with a better performance in the longitudinal component. The normal component values are close to the experimental value and within the measurement error by Sanquer (1998).

References

Bai, X. and Fuchs, L., 1994. Modeling of turbulent reactive flows past a bluff body: Assessment of accuracy and efficiency. Computers and Fluids, Vol. 23, No. 3, pp. 507-521.

Candel, S., 1992. Combustion instabilities coupled by pressure waves and their active control. 24th Symp.(Int.) on combustion.The Combustion Institute, pp. 1277-1296.

R. K. Cheng. Conditional sampling of turbulence intensities and reynolds stress in premixed turbulent flames. Combustion Science and Technology, 41:109-142, 1984.

R. K. Cheng, I. G. Shepherd, and I. Gokalp. A comparison of the velocity and scalar spectra in premixed flames. Combustion and Flame, 78:205-221, 1989.

R. K. Cheng and I. G. Shepherd. The influence of burner geometry on premixed turbulent flame propagation. Combustion and Flame, 85:7-26, 1991.

Dourado, W.C., 2003. Desenvolvimento de um método numérico em malhas não estructuradas hibridas para escoamentos turbulentos em baixo número de Mach: aplicação em chama propagando-se livremente e esteiras inertes e reativas. Ph.D. thesis, ITA, SJC-SP.

S. Fuji, M. Gomi, and M. Eguchi. Cold flow tests of a bluff-body flame stabilizer. Journal of Fluids Engineering, 100:323-330, 1978.

S. Fuji and M. Eguchi. A comparison of cold and reacting flows around a bluff - body flame stabilizer. Journal of Fluids Engineering, 103:328-333, 1981.

Fureby, C., Tabor, G. and Weller, H.G., 1997. Differential subgrid stress models in large eddy simulations. PHYS FLUIDS, Vol. 9, pp. 3578-3580.

Fureby, C., 2009. Les modeling of combustion for propulsion applications. Phil.Trans. R. Soc. A, Vol. 367, p. 2957.

Grinstein, F.F. and Kailasanath, K.K., 1994. Three dimensional numerical simulations of unsteady reactive square jets. Comb. and Flame, Vol. 100, p. 2.

Gulder, O.L., 1990. Turbulent premixed flame propagation models for different combustion regimes. Twenty-third Symposium (International) on Combustion.The Combustion Institute, Vol. Twenty-third Symposium, pp. 743-750.

G. R. Hertzberg, I. G. Shepherd, and L. Talbot. Vortex shedding behind rod stabilized flames. Combustion and Flame, 86(1):1-11, 1991.

Jayatilleke, C., 1969. The influence of prandtl number and surface roughness on the resistance of the laminar sublayer to momentum and heat transfer. Prog. Heat Mass Transfer, Vol. 1, pp. 193-321.

Kerstein, A. R., Linear-Eddy Modeling of Turbulent Transport II, Combustion and Flame, Vol. 75, 1989, pp. 397413.

Menon, S., McMurtry, P. A., and Kerstein, A. R., A Linear Eddy Mixing Model for Large Eddy Simulation of Turbulent Combustion, LES of Complex Engineering and Geophysical Flows. Ed. B. Galperin and S. Orszag, 1993.

Peters, N., 2000. Turbulent Combustion. Cambridge University Press, Cambridge.

Porumbel, I.,Menon S., 2006. Large Eddy Simulation of Bluff Body Stabilized Premixed Flame, AIAA 2006-152.

Sanquer, S., 1998. Experimental Study of a Buff-Body Wake, in Presence of Combustion, in Fully Developed Turbulent Channel Flow: Turbulence Scales and Critical Analysis of Transport and Combustion ModelsS. Ph.D. thesis, Universite de Poitiers, Potiers.

A. Sjunesson, R. Henriksson, and C. Lofstrom. Cars measurements and visualization of reacting flows in bluff body stabilized flame. AIAA - 92 - 3650, 1992

D. Veynante, J. M. Duclos, and J. Piana. Experimental analysis of flamelet models for premixed turbulent combustion. Twenty - Fifth Symposium (International) on Combustion, pages 1249-1256, 1994.

D. Veynante, J. Piana, J. M. Duclos, and C. Martel. Experimental analysis of flame surface density models for premixed turbulent combustion. Twenty - Sixth Symposium (Interna- tional) on Combustion, pages 1249-1256, 1996.

Veynante, D., 2006. Large eddy simulation of turbulent combustion. Conference on Turbulence and Interaction, Vol. TI2006, p. 20.

Weller, H.G., Marooney, C.J. and Gosman, A.D., 1990. A new spectral method for calculation of the time-varyng area of laminar flame in homogeneus turbulence. Twenty-third Symposium (International) on Combustion, The combustion institute, Vol. Twenty-third Symposium, pp. 629-636.

Weller, H.G., 1993. The development of a new flame area combustion model using conditional averagingThermo-Fluids Section Report TF 9307. Ph.D. thesis, Imperial College of Science, technology and Medicine, London.

Weller, H.G., Tabor, G., Gosman, A. and Fureby, C., 1998. Application of a flame-wrinkling les combustion model to a turbulent mixing layer. 27th Symposium (International) on Combustion The combustion Institute, Vol. 27th Symposium, pp. 899-907.

Weller, H.G. and Tabor, G., 2004. Large eddy simulation of premixed turbulent combustion using xi flame surface wrinkling model. flow,Turbulence and Combustion, Vol. 72, pp. 1-28.